



CERN-PH-EP-2013-095

LHCb-PAPER-2013-004

Oct. 1, 2013

Measurement of B meson production cross-sections in proton-proton collisions at $\sqrt{s} = 7$ TeV

The LHCb collaboration[†]

Abstract

The production cross-sections of B mesons are measured in pp collisions at a centre-of-mass energy of 7 TeV, using data collected with the LHCb detector corresponding to a integrated luminosity of 0.36 fb^{-1} . The B^+ , B^0 and B_s^0 mesons are reconstructed in the exclusive decays $B^+ \rightarrow J/\psi K^+$, $B^0 \rightarrow J/\psi K^{*0}$ and $B_s^0 \rightarrow J/\psi \phi$, with $J/\psi \rightarrow \mu^+ \mu^-$, $K^{*0} \rightarrow K^+ \pi^-$ and $\phi \rightarrow K^+ K^-$. The differential cross-sections are measured as functions of B meson transverse momentum p_T and rapidity y , in the range $0 < p_T < 40$ GeV/ c and $2.0 < y < 4.5$. The integrated cross-sections in the same p_T and y ranges, including charge-conjugate states, are measured to be

$$\begin{aligned}\sigma(pp \rightarrow B^+ + X) &= 38.9 \pm 0.3 \text{ (stat.)} \pm 2.5 \text{ (syst.)} \pm 1.3 \text{ (norm.) } \mu\text{b}, \\ \sigma(pp \rightarrow B^0 + X) &= 38.1 \pm 0.6 \text{ (stat.)} \pm 3.7 \text{ (syst.)} \pm 4.7 \text{ (norm.) } \mu\text{b}, \\ \sigma(pp \rightarrow B_s^0 + X) &= 10.5 \pm 0.2 \text{ (stat.)} \pm 0.8 \text{ (syst.)} \pm 1.0 \text{ (norm.) } \mu\text{b},\end{aligned}$$

where the third uncertainty arises from the pre-existing branching fraction measurements.

Submitted to JHEP

© CERN on behalf of the LHCb collaboration, license CC-BY-3.0.

[†]Authors are listed on the following pages.

LHCb collaboration

R. Aaij⁴⁰, C. Abellan Beteta^{35,n}, B. Adeva³⁶, M. Adinolfi⁴⁵, C. Adrover⁶, A. Affolder⁵¹, Z. Ajaltouni⁵, J. Albrecht⁹, F. Alessio³⁷, M. Alexander⁵⁰, S. Ali⁴⁰, G. Alkhazov²⁹, P. Alvarez Cartelle³⁶, A.A. Alves Jr^{24,37}, S. Amato², S. Amerio²¹, Y. Amhis⁷, L. Anderlini^{17,f}, J. Anderson³⁹, R. Andreassen⁵⁶, R.B. Appleby⁵³, O. Aquines Gutierrez¹⁰, F. Archilli¹⁸, A. Artamonov³⁴, M. Artuso⁵⁷, E. Aslanides⁶, G. Auriemma^{24,m}, S. Bachmann¹¹, J.J. Back⁴⁷, C. Baesso⁵⁸, V. Balagura³⁰, W. Baldini¹⁶, R.J. Barlow⁵³, C. Barschel³⁷, S. Barsuk⁷, W. Barter⁴⁶, Th. Bauer⁴⁰, A. Bay³⁸, J. Beddow⁵⁰, F. Bedeschi²², I. Bediaga¹, S. Belogurov³⁰, K. Belous³⁴, I. Belyaev³⁰, E. Ben-Haim⁸, M. Benayoun⁸, G. Bencivenni¹⁸, S. Benson⁴⁹, J. Benton⁴⁵, A. Berezhnoy³¹, R. Bernet³⁹, M.-O. Bettler⁴⁶, M. van Beuzekom⁴⁰, A. Bien¹¹, S. Bifani⁴⁴, T. Bird⁵³, A. Bizzeti^{17,h}, P.M. Bjørnstad⁵³, T. Blake³⁷, F. Blanc³⁸, J. Blouw¹¹, S. Blusk⁵⁷, V. Bocci²⁴, A. Bondar³³, N. Bondar²⁹, W. Bonivento¹⁵, S. Borghi⁵³, A. Borgia⁵⁷, T.J.V. Bowcock⁵¹, E. Bowen³⁹, C. Bozzi¹⁶, T. Brambach⁹, J. van den Brand⁴¹, J. Bressieux³⁸, D. Brett⁵³, M. Britsch¹⁰, T. Britton⁵⁷, N.H. Brook⁴⁵, H. Brown⁵¹, I. Burducea²⁸, A. Bursche³⁹, G. Busetto^{21,p}, J. Buytaert³⁷, S. Cadeddu¹⁵, O. Callot⁷, M. Calvi^{20,j}, M. Calvo Gomez^{35,n}, A. Camboni³⁵, P. Campana^{18,37}, D. Campora Perez³⁷, A. Carbone^{14,c}, G. Carboni^{23,k}, R. Cardinale^{19,i}, A. Cardini¹⁵, H. Carranza-Mejia⁴⁹, L. Carson⁵², K. Carvalho Akiba², G. Casse⁵¹, L. Castillo Garcia³⁷, M. Cattaneo³⁷, Ch. Cauet⁹, M. Charles⁵⁴, Ph. Charpentier³⁷, P. Chen^{3,38}, N. Chiapolini³⁹, M. Chrzaszcz²⁵, K. Ciba³⁷, X. Cid Vidal³⁷, G. Ciezarek⁵², P.E.L. Clarke⁴⁹, M. Clemencic³⁷, H.V. Cliff⁴⁶, J. Closier³⁷, C. Coca²⁸, V. Coco⁴⁰, J. Cogan⁶, E. Cogneras⁵, P. Collins³⁷, A. Comerma-Montells³⁵, A. Contu¹⁵, A. Cook⁴⁵, M. Coombes⁴⁵, S. Coquereau⁸, G. Corti³⁷, B. Couturier³⁷, G.A. Cowan⁴⁹, D.C. Craik⁴⁷, S. Cunliffe⁵², R. Currie⁴⁹, C. D'Ambrosio³⁷, P. David⁸, P.N.Y. David⁴⁰, I. De Bonis⁴, K. De Bruyn⁴⁰, S. De Capua⁵³, M. De Cian³⁹, J.M. De Miranda¹, L. De Paula², W. De Silva⁵⁶, P. De Simone¹⁸, D. Decamp⁴, M. Deckenhoff⁹, L. Del Buono⁸, D. Derkach¹⁴, O. Deschamps⁵, F. Dettori⁴¹, A. Di Canto¹¹, H. Dijkstra³⁷, M. Dogaru²⁸, S. Donleavy⁵¹, F. Dordet¹¹, A. Dosil Suárez³⁶, D. Dossett⁴⁷, A. Dovbnya⁴², F. Dupertuis³⁸, R. Dzhelyadin³⁴, A. Dziurda²⁵, A. Dzyuba²⁹, S. Easo^{48,37}, U. Egede⁵², V. Egorychev³⁰, S. Eidelman³³, D. van Eijk⁴⁰, S. Eisenhardt⁴⁹, U. Eitschberger⁹, R. Ekelhof⁹, L. Eklund^{50,37}, I. El Rifai⁵, Ch. Elsasser³⁹, D. Elsby⁴⁴, A. Falabella^{14,e}, C. Färber¹¹, G. Fardell⁴⁹, C. Farinelli⁴⁰, S. Farry¹², V. Fave³⁸, D. Ferguson⁴⁹, V. Fernandez Albor³⁶, F. Ferreira Rodrigues¹, M. Ferro-Luzzi³⁷, S. Filippov³², M. Fiore¹⁶, C. Fitzpatrick³⁷, M. Fontana¹⁰, F. Fontanelli^{19,i}, R. Forty³⁷, O. Francisco², M. Frank³⁷, C. Frei³⁷, M. Frosini^{17,f}, S. Furcas²⁰, E. Furfarò^{23,k}, A. Gallas Torreira³⁶, D. Galli^{14,c}, M. Gandelman², P. Gandini⁵⁷, Y. Gao³, J. Garofoli⁵⁷, P. Garosi⁵³, J. Garra Tico⁴⁶, L. Garrido³⁵, C. Gaspar³⁷, R. Gauld⁵⁴, E. Gersabeck¹¹, M. Gersabeck⁵³, T. Gershon^{47,37}, Ph. Ghez⁴, V. Gibson⁴⁶, V.V. Gligorov³⁷, C. Göbel⁵⁸, D. Golubkov³⁰, A. Golutvin^{52,30,37}, A. Gomes², H. Gordon⁵⁴, M. Grabalosa Gándara⁵, R. Graciani Diaz³⁵, L.A. Granado Cardoso³⁷, E. Graugés³⁵, G. Graziani¹⁷, A. Grecu²⁸, E. Greening⁵⁴, S. Gregson⁴⁶, O. Grünberg⁵⁹, B. Gui⁵⁷, E. Gushchin³², Yu. Guz^{34,37}, T. Gys³⁷, C. Hadjivasiliou⁵⁷, G. Haefeli³⁸, C. Haen³⁷, S.C. Haines⁴⁶, S. Hall⁵², T. Hampson⁴⁵, S. Hansmann-Menzemer¹¹, N. Harnew⁵⁴, S.T. Harnew⁴⁵, J. Harrison⁵³, T. Hartmann⁵⁹, J. He³⁷, V. Heijne⁴⁰, K. Hennessy⁵¹, P. Henrard⁵, J.A. Hernando Morata³⁶, E. van Herwijnen³⁷, A. Hicheur¹, E. Hicks⁵¹, D. Hill⁵⁴, M. Hoballah⁵, M. Holtrop⁴⁰, C. Hombach⁵³, P. Hopchev⁴, W. Hulsbergen⁴⁰, P. Hunt⁵⁴, T. Huse⁵¹, N. Hussain⁵⁴, D. Hutchcroft⁵¹, D. Hynds⁵⁰, V. Iakovenko⁴³, M. Idzik²⁶, P. Ilten¹², R. Jacobsson³⁷, A. Jaeger¹¹, E. Jans⁴⁰, P. Jaton³⁸, F. Jing³, M. John⁵⁴, D. Johnson⁵⁴,

C.R. Jones⁴⁶, C. Joram³⁷, B. Jost³⁷, M. Kaballo⁹, S. Kandybei⁴², M. Karacson³⁷,
 T.M. Karbach³⁷, I.R. Kenyon⁴⁴, U. Kerzel³⁷, T. Ketel⁴¹, A. Keune³⁸, B. Khanji²⁰,
 O. Kochebina⁷, I. Komarov³⁸, R.F. Koopman⁴¹, P. Koppenburg⁴⁰, M. Korolev³¹,
 A. Kozlinskiy⁴⁰, L. Kravchuk³², K. Kreplin¹¹, M. Kreps⁴⁷, G. Krocker¹¹, P. Krokovny³³,
 F. Kruse⁹, M. Kucharczyk^{20,25,j}, V. Kudryavtsev³³, T. Kvaratskheliya^{30,37}, V.N. La Thi³⁸,
 D. Lacarrere³⁷, G. Lafferty⁵³, A. Lai¹⁵, D. Lambert⁴⁹, R.W. Lambert⁴¹, E. Lanciotti³⁷,
 G. Lanfranchi^{18,37}, C. Langenbruch³⁷, T. Latham⁴⁷, C. Lazzeroni⁴⁴, R. Le Gac⁶,
 J. van Leerdam⁴⁰, J.-P. Lees⁴, R. Lefèvre⁵, A. Leflat³¹, J. Lefrançois⁷, S. Leo²², O. Leroy⁶,
 T. Lesiak²⁵, B. Leverington¹¹, Y. Li³, L. Li Gioi⁵, M. Liles⁵¹, R. Lindner³⁷, C. Linn¹¹, B. Liu³,
 G. Liu³⁷, S. Lohn³⁷, I. Longstaff⁵⁰, J.H. Lopes², E. Lopez Asamar³⁵, N. Lopez-March³⁸, H. Lu³,
 D. Lucchesi^{21,p}, J. Luisier³⁸, H. Luo⁴⁹, F. Machefert⁷, I.V. Machikhiliyan^{4,30}, F. Maciuc²⁸,
 O. Maev^{29,37}, S. Malde⁵⁴, G. Manca^{15,d}, G. Mancinelli⁶, U. Marconi¹⁴, R. Märki³⁸, J. Marks¹¹,
 G. Martellotti²⁴, A. Martens⁸, A. Martín Sánchez⁷, M. Martinelli⁴⁰, D. Martinez Santos⁴¹,
 D. Martins Tostes², A. Massafferri¹, R. Matev³⁷, Z. Mathe³⁷, C. Matteuzzi²⁰, E. Maurice⁶,
 A. Mazurov^{16,32,37,e}, J. McCarthy⁴⁴, A. McNab⁵³, R. McNulty¹², B. Meadows^{56,54}, F. Meier⁹,
 M. Meissner¹¹, M. Merk⁴⁰, D.A. Milanes⁸, M.-N. Minard⁴, J. Molina Rodriguez⁵⁸, S. Monteil⁵,
 D. Moran⁵³, P. Morawski²⁵, M.J. Morello^{22,r}, R. Mountain⁵⁷, I. Mous⁴⁰, F. Muheim⁴⁹,
 K. Müller³⁹, R. Muresan²⁸, B. Muryn²⁶, B. Muster³⁸, P. Naik⁴⁵, T. Nakada³⁸,
 R. Nandakumar⁴⁸, I. Nasteva¹, M. Needham⁴⁹, N. Neufeld³⁷, A.D. Nguyen³⁸, T.D. Nguyen³⁸,
 C. Nguyen-Mau^{38,o}, M. Nicol⁷, V. Niess⁵, R. Niet⁹, N. Nikitin³¹, T. Nikodem¹¹,
 A. Nomerotski⁵⁴, A. Novoselov³⁴, A. Oblakowska-Mucha²⁶, V. Obraztsov³⁴, S. Oggero⁴⁰,
 S. Ogilvy⁵⁰, O. Okhrimenko⁴³, R. Oldeman^{15,d}, M. Orlandea²⁸, J.M. Otalora Goicochea²,
 P. Owen⁵², A. Oyanguren³⁵, B.K. Pal⁵⁷, A. Palano^{13,b}, M. Palutan¹⁸, J. Panman³⁷,
 A. Papanestis⁴⁸, M. Pappagallo⁵⁰, C. Parkes⁵³, C.J. Parkinson⁵², G. Passaleva¹⁷, G.D. Patel⁵¹,
 M. Patel⁵², G.N. Patrick⁴⁸, C. Patrignani^{19,i}, C. Pavel-Nicorescu²⁸, A. Pazos Alvarez³⁶,
 A. Pellegrino⁴⁰, G. Penso^{24,l}, M. Pepe Altarelli³⁷, S. Perazzini^{14,c}, D.L. Perego^{20,j},
 E. Perez Trigo³⁶, A. Pérez-Calero Yzquierdo³⁵, P. Perret⁵, M. Perrin-Terrin⁶, G. Pessina²⁰,
 K. Petridis⁵², A. Petrolini^{19,i}, A. Phan⁵⁷, E. Picatoste Olloqui³⁵, B. Pietrzyk⁴, T. Pilarčík⁴⁷,
 D. Pinci²⁴, S. Playfer⁴⁹, M. Plo Casasus³⁶, F. Polci⁸, G. Polok²⁵, A. Poluektov^{47,33},
 E. Polycarpo², D. Popov¹⁰, B. Popovici²⁸, C. Potterat³⁵, A. Powell⁵⁴, J. Prisciandaro³⁸,
 A. Pritchard⁵¹, C. Prouve⁷, V. Pugatch⁴³, A. Puig Navarro³⁸, G. Punzi^{22,q}, W. Qian⁴,
 J.H. Rademacker⁴⁵, B. Rakotomiaramanana³⁸, M.S. Rangel², I. Raniuk⁴², N. Rauschmayr³⁷,
 G. Raven⁴¹, S. Redford⁵⁴, M.M. Reid⁴⁷, A.C. dos Reis¹, S. Ricciardi⁴⁸, A. Richards⁵²,
 K. Rinnert⁵¹, V. Rives Molina³⁵, D.A. Roa Romero⁵, P. Robbe⁷, E. Rodrigues⁵³,
 P. Rodriguez Perez³⁶, S. Roiser³⁷, V. Romanovsky³⁴, A. Romero Vidal³⁶, J. Rouvinet³⁸,
 T. Ruf³⁷, F. Ruffini²², H. Ruiz³⁵, P. Ruiz Valls³⁵, G. Sabatino^{24,k}, J.J. Saborido Silva³⁶,
 N. Sagidova²⁹, P. Sail⁵⁰, B. Saitta^{15,d}, C. Salzmann³⁹, B. Sanmartin Sedes³⁶, M. Sannino^{19,i},
 R. Santacesaria²⁴, C. Santamarina Rios³⁶, E. Santovetti^{23,k}, M. Sapunov⁶, A. Sarti^{18,l},
 C. Satriano^{24,m}, A. Satta²³, M. Savrie^{16,e}, D. Savrina^{30,31}, P. Schaack⁵², M. Schiller⁴¹,
 H. Schindler³⁷, M. Schlupp⁹, M. Schmelling¹⁰, B. Schmidt³⁷, O. Schneider³⁸, A. Schopper³⁷,
 M.-H. Schune⁷, R. Schwemmer³⁷, B. Sciascia¹⁸, A. Sciubba²⁴, M. Seco³⁶, A. Semennikov³⁰,
 I. Sepp⁵², N. Serra³⁹, J. Serrano⁶, P. Seyfert¹¹, M. Shapkin³⁴, I. Shapoval^{16,42}, P. Shatalov³⁰,
 Y. Shcheglov²⁹, T. Shears^{51,37}, L. Shekhtman³³, O. Shevchenko⁴², V. Shevchenko³⁰, A. Shires⁵²,
 R. Silva Coutinho⁴⁷, T. Skwarnicki⁵⁷, N.A. Smith⁵¹, E. Smith^{54,48}, M. Smith⁵³, M.D. Sokoloff⁵⁶,
 F.J.P. Soler⁵⁰, F. Soomro¹⁸, D. Souza⁴⁵, B. Souza De Paula², B. Spaan⁹, A. Sparkes⁴⁹,
 P. Spradlin⁵⁰, F. Stagni³⁷, S. Stahl¹¹, O. Steinkamp³⁹, S. Stoica²⁸, S. Stone⁵⁷, B. Storaci³⁹,

M. Straticiuc²⁸, U. Straumann³⁹, V.K. Subbiah³⁷, S. Swientek⁹, V. Syropoulos⁴¹,
M. Szczekowski²⁷, P. Szczypka^{38,37}, T. Szumlak²⁶, S. T'Jampens⁴, M. Teklishyn⁷,
E. Teodorescu²⁸, F. Teubert³⁷, C. Thomas⁵⁴, E. Thomas³⁷, J. van Tilburg¹¹, V. Tisserand⁴,
M. Tobin³⁸, S. Tolk⁴¹, D. Tonelli³⁷, S. Topp-Joergensen⁵⁴, N. Torr⁵⁴, E. Tournefier^{4,52},
S. Tourneur³⁸, M.T. Tran³⁸, M. Tresch³⁹, A. Tsaregorodtsev⁶, P. Tsopelas⁴⁰, N. Tuning⁴⁰,
M. Ubeda Garcia³⁷, A. Ukleja²⁷, D. Urner⁵³, U. Uwer¹¹, V. Vagnoni¹⁴, G. Valenti¹⁴,
R. Vazquez Gomez³⁵, P. Vazquez Regueiro³⁶, S. Vecchi¹⁶, J.J. Velthuis⁴⁵, M. Veltri^{17,g},
G. Veneziano³⁸, M. Vesterinen³⁷, B. Viaud⁷, D. Vieira², X. Vilasis-Cardona^{35,n}, A. Vollhardt³⁹,
D. Volyansky¹⁰, D. Voong⁴⁵, A. Vorobyev²⁹, V. Vorobyev³³, C. Voß⁵⁹, H. Voss¹⁰, R. Waldi⁵⁹,
R. Wallace¹², S. Wandernoth¹¹, J. Wang⁵⁷, D.R. Ward⁴⁶, N.K. Watson⁴⁴, A.D. Webber⁵³,
D. Websdale⁵², M. Whitehead⁴⁷, J. Wicht³⁷, J. Wiechczynski²⁵, D. Wiedner¹¹, L. Wiggers⁴⁰,
G. Wilkinson⁵⁴, M.P. Williams^{47,48}, M. Williams⁵⁵, F.F. Wilson⁴⁸, J. Wishahi⁹, M. Witek²⁵,
S.A. Wotton⁴⁶, S. Wright⁴⁶, S. Wu³, K. Wyllie³⁷, Y. Xie^{49,37}, Z. Xing⁵⁷, Z. Yang³, R. Young⁴⁹,
X. Yuan³, O. Yushchenko³⁴, M. Zangoli¹⁴, M. Zavertyaev^{10,a}, F. Zhang³, L. Zhang⁵⁷,
W.C. Zhang¹², Y. Zhang³, A. Zhelezov¹¹, A. Zhokhov³⁰, L. Zhong³, A. Zvyagin³⁷.

¹*Centro Brasileiro de Pesquisas Físicas (CBPF), Rio de Janeiro, Brazil*

²*Universidade Federal do Rio de Janeiro (UFRJ), Rio de Janeiro, Brazil*

³*Center for High Energy Physics, Tsinghua University, Beijing, China*

⁴*LAPP, Université de Savoie, CNRS/IN2P3, Annecy-Le-Vieux, France*

⁵*Clermont Université, Université Blaise Pascal, CNRS/IN2P3, LPC, Clermont-Ferrand, France*

⁶*CPPM, Aix-Marseille Université, CNRS/IN2P3, Marseille, France*

⁷*LAL, Université Paris-Sud, CNRS/IN2P3, Orsay, France*

⁸*LPNHE, Université Pierre et Marie Curie, Université Paris Diderot, CNRS/IN2P3, Paris, France*

⁹*Fakultät Physik, Technische Universität Dortmund, Dortmund, Germany*

¹⁰*Max-Planck-Institut für Kernphysik (MPIK), Heidelberg, Germany*

¹¹*Physikalisches Institut, Ruprecht-Karls-Universität Heidelberg, Heidelberg, Germany*

¹²*School of Physics, University College Dublin, Dublin, Ireland*

¹³*Sezione INFN di Bari, Bari, Italy*

¹⁴*Sezione INFN di Bologna, Bologna, Italy*

¹⁵*Sezione INFN di Cagliari, Cagliari, Italy*

¹⁶*Sezione INFN di Ferrara, Ferrara, Italy*

¹⁷*Sezione INFN di Firenze, Firenze, Italy*

¹⁸*Laboratori Nazionali dell'INFN di Frascati, Frascati, Italy*

¹⁹*Sezione INFN di Genova, Genova, Italy*

²⁰*Sezione INFN di Milano Bicocca, Milano, Italy*

²¹*Sezione INFN di Padova, Padova, Italy*

²²*Sezione INFN di Pisa, Pisa, Italy*

²³*Sezione INFN di Roma Tor Vergata, Roma, Italy*

²⁴*Sezione INFN di Roma La Sapienza, Roma, Italy*

²⁵*Henryk Niewodniczanski Institute of Nuclear Physics Polish Academy of Sciences, Kraków, Poland*

²⁶*AGH - University of Science and Technology, Faculty of Physics and Applied Computer Science, Kraków, Poland*

²⁷*National Center for Nuclear Research (NCBJ), Warsaw, Poland*

²⁸*Horia Hulubei National Institute of Physics and Nuclear Engineering, Bucharest-Magurele, Romania*

²⁹*Petersburg Nuclear Physics Institute (PNPI), Gatchina, Russia*

³⁰*Institute of Theoretical and Experimental Physics (ITEP), Moscow, Russia*

³¹*Institute of Nuclear Physics, Moscow State University (SINP MSU), Moscow, Russia*

³²*Institute for Nuclear Research of the Russian Academy of Sciences (INR RAN), Moscow, Russia*

³³*Budker Institute of Nuclear Physics (SB RAS) and Novosibirsk State University, Novosibirsk, Russia*

- ³⁴*Institute for High Energy Physics (IHEP), Protvino, Russia*
- ³⁵*Universitat de Barcelona, Barcelona, Spain*
- ³⁶*Universidad de Santiago de Compostela, Santiago de Compostela, Spain*
- ³⁷*European Organization for Nuclear Research (CERN), Geneva, Switzerland*
- ³⁸*Ecole Polytechnique Fédérale de Lausanne (EPFL), Lausanne, Switzerland*
- ³⁹*Physik-Institut, Universität Zürich, Zürich, Switzerland*
- ⁴⁰*Nikhef National Institute for Subatomic Physics, Amsterdam, The Netherlands*
- ⁴¹*Nikhef National Institute for Subatomic Physics and VU University Amsterdam, Amsterdam, The Netherlands*
- ⁴²*NSC Kharkiv Institute of Physics and Technology (NSC KIPT), Kharkiv, Ukraine*
- ⁴³*Institute for Nuclear Research of the National Academy of Sciences (KINR), Kyiv, Ukraine*
- ⁴⁴*University of Birmingham, Birmingham, United Kingdom*
- ⁴⁵*H.H. Wills Physics Laboratory, University of Bristol, Bristol, United Kingdom*
- ⁴⁶*Cavendish Laboratory, University of Cambridge, Cambridge, United Kingdom*
- ⁴⁷*Department of Physics, University of Warwick, Coventry, United Kingdom*
- ⁴⁸*STFC Rutherford Appleton Laboratory, Didcot, United Kingdom*
- ⁴⁹*School of Physics and Astronomy, University of Edinburgh, Edinburgh, United Kingdom*
- ⁵⁰*School of Physics and Astronomy, University of Glasgow, Glasgow, United Kingdom*
- ⁵¹*Oliver Lodge Laboratory, University of Liverpool, Liverpool, United Kingdom*
- ⁵²*Imperial College London, London, United Kingdom*
- ⁵³*School of Physics and Astronomy, University of Manchester, Manchester, United Kingdom*
- ⁵⁴*Department of Physics, University of Oxford, Oxford, United Kingdom*
- ⁵⁵*Massachusetts Institute of Technology, Cambridge, MA, United States*
- ⁵⁶*University of Cincinnati, Cincinnati, OH, United States*
- ⁵⁷*Syracuse University, Syracuse, NY, United States*
- ⁵⁸*Pontifícia Universidade Católica do Rio de Janeiro (PUC-Rio), Rio de Janeiro, Brazil, associated to ²*
- ⁵⁹*Institut für Physik, Universität Rostock, Rostock, Germany, associated to ¹¹*
- ^a*P.N. Lebedev Physical Institute, Russian Academy of Science (LPI RAS), Moscow, Russia*
- ^b*Università di Bari, Bari, Italy*
- ^c*Università di Bologna, Bologna, Italy*
- ^d*Università di Cagliari, Cagliari, Italy*
- ^e*Università di Ferrara, Ferrara, Italy*
- ^f*Università di Firenze, Firenze, Italy*
- ^g*Università di Urbino, Urbino, Italy*
- ^h*Università di Modena e Reggio Emilia, Modena, Italy*
- ⁱ*Università di Genova, Genova, Italy*
- ^j*Università di Milano Bicocca, Milano, Italy*
- ^k*Università di Roma Tor Vergata, Roma, Italy*
- ^l*Università di Roma La Sapienza, Roma, Italy*
- ^m*Università della Basilicata, Potenza, Italy*
- ⁿ*LIFAELS, La Salle, Universitat Ramon Llull, Barcelona, Spain*
- ^o*Hanoi University of Science, Hanoi, Viet Nam*
- ^p*Università di Padova, Padova, Italy*
- ^q*Università di Pisa, Pisa, Italy*
- ^r*Scuola Normale Superiore, Pisa, Italy*

1 Introduction

Measurements of beauty production in multi-TeV proton-proton (pp) collisions at the LHC provide important tests of quantum chromodynamics. State of the art theoretical predictions are given by the fixed-order plus next-to-leading logarithm (FONLL) approach [1, 2, 3]. In these calculations, the dominant uncertainties arise from the choice of the renormalisation and factorisation scales, and the assumed b -quark mass [4]. The primary products of $b\bar{b}$ hadronisation are B^+ , B^0 , B_s^0 and their charge-conjugate states (throughout the paper referred to as B mesons) formed by one \bar{b} quark bound to one of the three light quarks (u , d and s). Accurate measurements of the cross-sections probe the validity of the production models. At the LHC, $b\bar{b}$ production has been studied in inclusive $b \rightarrow J/\psi X$ decays [5, 6] and semileptonic [7, 8] decays. Other measurements, using fully reconstructed B mesons, have also been performed by the LHCb and CMS collaborations [9, 10, 11, 12].

In this paper, a measurement of the production cross-sections of B mesons (including their charge-conjugate states) is presented. This study is performed in the transverse momentum range $0 < p_T < 40$ GeV/ c and rapidity range $2.0 < y < 4.5$ using data, corresponding to a integrated luminosity of 0.36 fb^{-1} , collected in pp collisions at centre-of-mass energy of 7 TeV by the LHCb experiment. The B mesons are reconstructed in the exclusive decays $B^+ \rightarrow J/\psi K^+$, $B^0 \rightarrow J/\psi K^{*0}$ and $B_s^0 \rightarrow J/\psi \phi$, with $J/\psi \rightarrow \mu^+\mu^-$, $K^{*0} \rightarrow K^+\pi^-$ and $\phi \rightarrow K^+K^-$.

The LHCb detector [13] is a single-arm forward spectrometer covering the pseudorapidity range $2 < \eta < 5$, designed for the study of particles containing b or c quarks. The detector includes a high-precision tracking system consisting of a silicon-strip vertex detector surrounding the pp interaction region, a large-area silicon-strip detector located upstream of a dipole magnet with a bending power of about 4 Tm, and three stations of silicon-strip detectors and straw drift tubes placed downstream. The combined tracking system has momentum resolution $\Delta p/p$ that varies from 0.4% at 5 GeV/ c to 0.6% at 100 GeV/ c , and impact parameter resolution better than 20 μm for transverse momentum higher than 3 GeV/ c . Charged hadrons are identified using two ring-imaging Cherenkov (RICH) detectors. Photon, electron and hadron candidates are identified by a calorimeter system consisting of scintillating-pad and preshower detectors, an electromagnetic calorimeter and a hadronic calorimeter. Muons are identified by a system composed of alternating layers of iron and multiwire proportional chambers.

The events used in this analysis are selected by a two-stage trigger system [14]. The first stage is hardware based whilst the second stage is software based. At the hardware stage events containing either a single muon or a pair of muon candidates, with high transverse momentum, are selected. In the subsequent software trigger the decision of the single-muon or dimuon hardware trigger is confirmed and a muon pair with an invariant mass consistent with the known J/ψ mass [15] is required. To reject high-multiplicity events with a large number of pp interactions, global event cuts on the hit multiplicities of subdetectors are applied.

2 Candidate selection

The selection of B meson candidates starts by forming $J/\psi \rightarrow \mu^+ \mu^-$ decay candidates. These are formed from pairs of oppositely-charged particles that are identified as muons and have $p_T > 0.7 \text{ GeV}/c$. Good quality of the reconstructed tracks is ensured by requiring the χ^2/ndf of the track fit to be less than 4, where ndf is the number of degrees of freedom of the fit. The muon candidates are required to originate from a common vertex and the χ^2/ndf of the vertex fit is required to be less than 9. The mass of the J/ψ candidate is required to be around the known J/ψ mass [15], between 3.04 and $3.14 \text{ GeV}/c^2$.

Kaons used to form $B^+ \rightarrow J/\psi K^+$ candidates are required to have p_T larger than $0.5 \text{ GeV}/c$. Information from the RICH detector system is not used in the selection since the $B^+ \rightarrow J/\psi \pi^+$ decay is Cabibbo suppressed. Candidates for $K^{*0} \rightarrow K^+ \pi^-$ and $\phi \rightarrow K^+ K^-$ decays are formed from pairs of oppositely-charged hadron candidates. Since the background levels of these two channels are higher than for $B^+ \rightarrow J/\psi K^+$ decay, the hadron identification information provided by the RICH detectors is used. Kaons used to form K^{*0} candidates in the $B^0 \rightarrow J/\psi K^{*0}$ channel and ϕ candidates in the $B_s^0 \rightarrow J/\psi \phi$ channel are selected by cutting on the difference between the log-likelihoods of the kaon and pion hypotheses provided by the RICH detectors ($\text{DLL}_{K\pi} > 0$). The pions used to form K^{*0} candidates are required to be inconsistent with the kaon hypothesis ($\text{DLL}_{\pi K} > -5$). The same track quality cuts used for muons are applied to kaons and pions. The K^{*0} and ϕ meson candidates are constructed requiring a good vertex quality ($\chi^2/\text{ndf} < 16$) and $p_T > 1.0 \text{ GeV}/c$. The masses of the K^{*0} and ϕ candidates are required to be consistent with their known masses [15], in the intervals $0.826 - 0.966 \text{ GeV}/c^2$ and $1.008 - 1.032 \text{ GeV}/c^2$, respectively.

The J/ψ candidate is combined with a K^+ , K^{*0} or ϕ candidate to form a B^+ , B^0 or B_s^0 meson, respectively. A vertex fit [16] is performed that constrains the daughter particles to originate from a common point and the mass of the muon pair to match the known J/ψ mass [15]. The χ^2/ndf returned by this fit is required to be less than 9. To further reduce the combinatorial background due to particles produced in the primary pp interaction, only B candidates with a decay time larger than 0.3 ps , which corresponds to about 6 times the decay time resolution, are kept. In the $B^0 \rightarrow J/\psi K^{*0}$ samples, duplicate candidates are found that share the same J/ψ particle but have pion tracks that are reconstructed several times from one track. In these cases only one of the candidates is randomly retained. Duplicate candidates of other sources in the other decay modes occur at a much lower rate and are retained. Finally, the fiducial requirements $0 < p_T < 40 \text{ GeV}/c$ and $2.0 < y < 4.5$ are applied to the B meson candidates.

3 Cross-section determination

The differential production cross-section for each B meson species is calculated as

$$\frac{d^2\sigma(B)}{dp_T \, dy} = \frac{N_B(p_T, y)}{\epsilon_{\text{tot}}(p_T, y) \, \mathcal{L}_{\text{int}} \, \mathcal{B}(B \rightarrow J/\psi X) \, \Delta p_T \, \Delta y},$$

where $N_B(p_T, y)$ is the number of reconstructed signal candidates in a given (p_T, y) bin, $\epsilon_{\text{tot}}(p_T, y)$ is the total efficiency in a given (p_T, y) bin, \mathcal{L}_{int} is the integrated luminosity, $\mathcal{B}(B \rightarrow J/\psi X)$ is the product of the branching fractions of the decays in the complete decay chain, and Δp_T and Δy are the widths of the bin. The width of each y bin is fixed to 0.5 while the widths of the p_T bins vary to allow for sufficient number of candidates in each bin.

The signal yield in each bin of p_T and y is determined using an extended unbinned maximum likelihood fit to the invariant mass distribution of the reconstructed B candidates. The fit model includes two components: a double-sided Crystal Ball function to model the signal and an exponential function to model the combinatorial background. The former is an extension of the Crystal Ball function [17] that has tails on both the low- and the high-mass side of the peak described by separate parameters, which are determined from simulation. For the B^+ channel, the $K\pi$ misidentified $B^+ \rightarrow J/\psi \pi^+$ decay is modelled by a shape that is found to fit the distribution of simulated events. The invariant mass distributions of the selected B candidates and the fit results in one p_T and y bin are shown in Fig. 1.

For the $B^0 \rightarrow J/\psi K^{*0}$ and $B_s^0 \rightarrow J/\psi \phi$ decay channels, an additional non-resonant S-wave component (where the $K^+\pi^-$ and the K^+K^- originate directly from B^0 and B_s^0 decays, and not via K^{*0} or ϕ resonances) is also present. The amount of this component present in each case is determined from an independent fit to the $K^+\pi^-$ or K^+K^- mass distribution, respectively, integrating the p_T and y range. The signal component is described by a relativistic Breit-Wigner function, and the S-wave background by a phase space function. From the fit results, the S-wave fractions are determined to be $\sim 6\%$ for $B^0 \rightarrow J/\psi K^+\pi^-$ and $\sim 3\%$ for $B_s^0 \rightarrow J/\psi K^+K^-$ decays. The yields of B mesons are then corrected according to the S-wave fractions.

The geometrical acceptance as well as the reconstruction and selection efficiencies, except for the hadron identification efficiencies, are determined using simulated signal events. The pp collisions are generated using PYTHIA 6.4 [18] with a specific LHCb configuration [19]. Decays of hadronic particles are described by EVTGEN [20], in which final state radiation is generated using PHOTOS [21]. The interaction of the generated particles with the detector and its response are implemented using the GEANT4 toolkit [22] as described in Ref. [23]. The hadron identification efficiencies are measured using tracks from the decay $D^{*+} \rightarrow D^0\pi^+$ with $D^0 \rightarrow K^-\pi^+$, selected without using information from the RICH detectors [24].

Only candidates where the J/ψ is responsible for the trigger decision are used. The trigger efficiency is measured in data using the tag and probe method described in Ref. [14].

The luminosity is measured using Van der Meer scans and a beam-gas imaging method [25]. The integrated luminosity of the data sample used in this analysis is determined to be $362 \pm 13 \text{ pb}^{-1}$.

The branching fraction $\mathcal{B}(B^0 \rightarrow J/\psi K^{*0})$ measured by the Belle collaboration [26] is used in the determination of the B^0 cross-section, since it includes the effect of the S-wave interference, while other measurements do not. The measurement of $\mathcal{B}(B_s^0 \rightarrow J/\psi \phi)$ given in Ref. [27] is used in the determination of the B_s^0 cross-section. Since this branching fraction

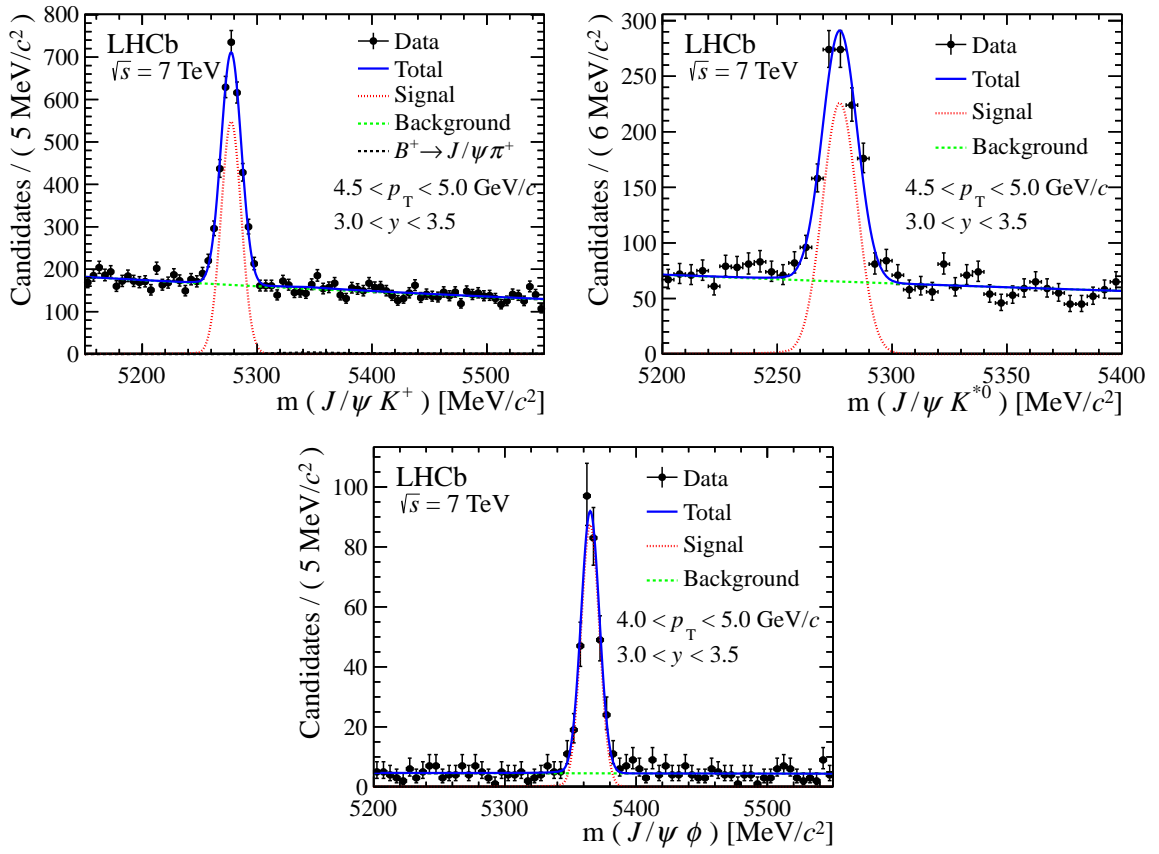


Figure 1: Invariant mass distributions of the selected candidates for (*top left*) B^+ and (*top right*) B^0 decays, both in the range $4.5 < p_T < 5.0 \text{ GeV}/c$, $3.0 < y < 3.5$, and (*bottom*) B_s^0 decay in the range $4.0 < p_T < 5.0 \text{ GeV}/c$, $3.0 < y < 3.5$. The results of the fit to the model described in the text are superimposed. The Cabibbo-suppressed background is barely visible in the top left plot.

measurement used the average ratio of fragmentation fractions f_s/f_d from Ref. [28, 29], the result in this paper cannot be taken as an independent measurement of f_s/f_d . The other branching fractions are obtained from Ref. [15].

4 Systematic uncertainties

The measurements are affected by systematic uncertainties in the determination of the signal yields, efficiencies, branching fractions and luminosity, as summarised in Table 1. The total systematic uncertainty is obtained from the sum in quadrature of all contributions.

Uncertainties on the signal yields arise from imperfect knowledge of the signal shape, non-resonant background and finite size of the bins. The uncertainty from the signal shape is estimated by comparing the fitted and generated signal yields in simulation. The non-resonant background ratios determined in this analysis are compared with those from measurements with angular fits [27] and the differences are assigned as systematic

Table 1: Relative systematic uncertainties (in %), given as single values or as ranges, when they depend on the (p_T , y) bin.

Source	B^+	B^0	B_s^0
Signal fit model	2.5	1.3	1.2
Fit range	0.1	1.0	0.4
Non-resonant background	-	2.2	1.9
Combinatorial background	0.6	0.8	0.3
Bin size	$0.1 - 10.9$	$0.1 - 19.3$	$0.1 - 13.2$
Duplicate candidates	-	3.1	-
Trigger efficiency	$2.4 - 7.9$	$2.6 - 7.9$	$2.6 - 6.5$
Tracking efficiency	$2.4 - 7.4$	$4.4 - 8.3$	$4.4 - 8.5$
Vertex quality cut	1.0	0.9	0.2
Muon identification	$0.7 - 4.9$	$0.8 - 5.0$	$0.8 - 5.8$
Hadron identification	-	1.0	0.8
Angular distribution	-	$0.1 - 0.3$	$0.1 - 4.7$
p_T distribution	-	$0 - 24.4$	-
Branching fractions	3.3	12.3	10.0
Luminosity	3.5	3.5	3.5

uncertainties. By varying the p_T or y binning, the uncertainty for changing the binning in p_T is found to be small while that for y is non-negligible in the low y bin. An uncertainty is assigned due to the procedure of removal of duplicate candidates in $B^0 \rightarrow J/\psi K^{*0}$ events. For the other modes this effect is found to be negligible. The uncertainties from the background shape, misidentified $B^+ \rightarrow J/\psi \pi^+$ background and mass fit range are small.

Uncertainties on the efficiencies arise from the trigger, tracking, particle identification, angular distribution, p_T spectrum and vertex fit quality cut. The systematic uncertainty from the trigger efficiency is evaluated by comparing the efficiency measured using a trigger-unbiased sample of simulated J/ψ events with that determined from the simulation. The effect of the global event cuts in the trigger is found to be negligible. The tracking efficiencies are estimated with a tag and probe method [30] using $J/\psi \rightarrow \mu^+ \mu^-$ events in both data and simulation. The simulated efficiencies, used to determine the cross-section, are corrected according to the differences between data and simulation. The tracking uncertainty includes two components: the first is from the data-simulation difference correction; the second is due to the uncertainty on the hadronic interaction length of the detector used in the simulation. Possible systematic biases in the determination of the

hadron identification efficiency are estimated using simulated events and comparing the true efficiency with that obtained by applying the same procedure as for the data. The muon identification uncertainty is estimated by comparing the efficiency in simulation with that measured, on data, using a tag and probe method. The systematic uncertainties due to the uncertainties on the angular distributions of B^0 and B_s^0 decays [15, 31] are taken into account by simulating the effect of varying the central values of the polarization amplitudes by ± 1 sigma. In the first p_T bin of the B^0 sample, the agreement of the p_T distributions between data and simulation is not as good as in the other bins. The discrepancy is assigned as an additional uncertainty for that bin. The vertex fit quality cut uncertainty is estimated from the data to simulation comparison. By calculating the signal yields and efficiencies separately for data taken with two magnet polarities, the results are found to be stable.

The systematic uncertainties from the branching fractions are calculated with their correlations taken into account. Since the $\mathcal{B}(B^0 \rightarrow J/\psi K^{*0})$ and $\mathcal{B}(B_s^0 \rightarrow J/\psi \phi)$ have been measured with sizeable uncertainty, the corresponding uncertainties are listed separately in the cross-section results. The absolute luminosity scale is measured with 3.5% uncertainty, which is dominated by the beam current uncertainty [25].

5 Results and conclusion

The measured differential production cross-sections of B mesons in bins of p_T and y are shown in Fig. 2. These results are integrated separately over y and p_T , and compared with the FONLL predictions [3], as shown in Fig. 3 and Fig. 4, respectively. The hadronisation fractions $f_u = f_d = (33.7 \pm 2.2)\%$ and $f_s = (9.0 \pm 0.9)\%$ from Ref. [28] are used to fix the overall scale of FONLL. The uncertainty of the FONLL computation includes the uncertainties on the b -quark mass, renormalisation and factorisation scales, and CTEQ 6.6 [32] parton distribution functions. Good agreement is seen between the FONLL predictions and measured data.

The integrated cross-sections of the B mesons with $0 < p_T < 40$ GeV/ c and $2.0 < y < 4.5$ are

$$\begin{aligned}\sigma(pp \rightarrow B^+ X) &= 38.9 \pm 0.3 \text{ (stat.)} \pm 2.5 \text{ (syst.)} \pm 1.3 \text{ (norm.) } \mu\text{b}, \\ \sigma(pp \rightarrow B^0 X) &= 38.1 \pm 0.6 \text{ (stat.)} \pm 3.7 \text{ (syst.)} \pm 4.7 \text{ (norm.) } \mu\text{b}, \\ \sigma(pp \rightarrow B_s^0 X) &= 10.5 \pm 0.2 \text{ (stat.)} \pm 0.8 \text{ (syst.)} \pm 1.0 \text{ (norm.) } \mu\text{b},\end{aligned}$$

where the third uncertainties arise from the uncertainties of the branching fractions used for normalisation. The B^+ result is in good agreement with a previous measurement by LHCb [9]. These represent the first measurements of B^0 and B_s^0 meson production cross-sections in pp collisions in the forward region at centre-of-mass energy of 7 TeV.

Acknowledgements

We thank M. Cacciari for providing the FONLL predictions for the B meson production cross-sections. We express our gratitude to our colleagues in the CERN accelerator departments for the excellent performance of the LHC. We thank the technical and administrative staff at the LHCb institutes. We acknowledge support from CERN and from the national agencies: CAPES, CNPq, FAPERJ and FINEP (Brazil); NSFC (China); CNRS/IN2P3 and Region Auvergne (France); BMBF, DFG, HGF and MPG (Germany); SFI (Ireland); INFN (Italy); FOM and NWO (The Netherlands); SCSR (Poland); ANCS/IFA (Romania); MinES, Rosatom, RFBR and NRC “Kurchatov Institute” (Russia); MinECo, XuntaGal and GENCAT (Spain); SNSF and SER (Switzerland); NAS Ukraine (Ukraine); STFC (United Kingdom); NSF (USA). We also acknowledge the support received from the ERC under FP7. The Tier1 computing centres are supported by IN2P3 (France), KIT and BMBF (Germany), INFN (Italy), NWO and SURF (The Netherlands), PIC (Spain), GridPP (United Kingdom). We are thankful for the computing resources put at our disposal by Yandex LLC (Russia), as well as to the communities behind the multiple open source software packages that we depend on.

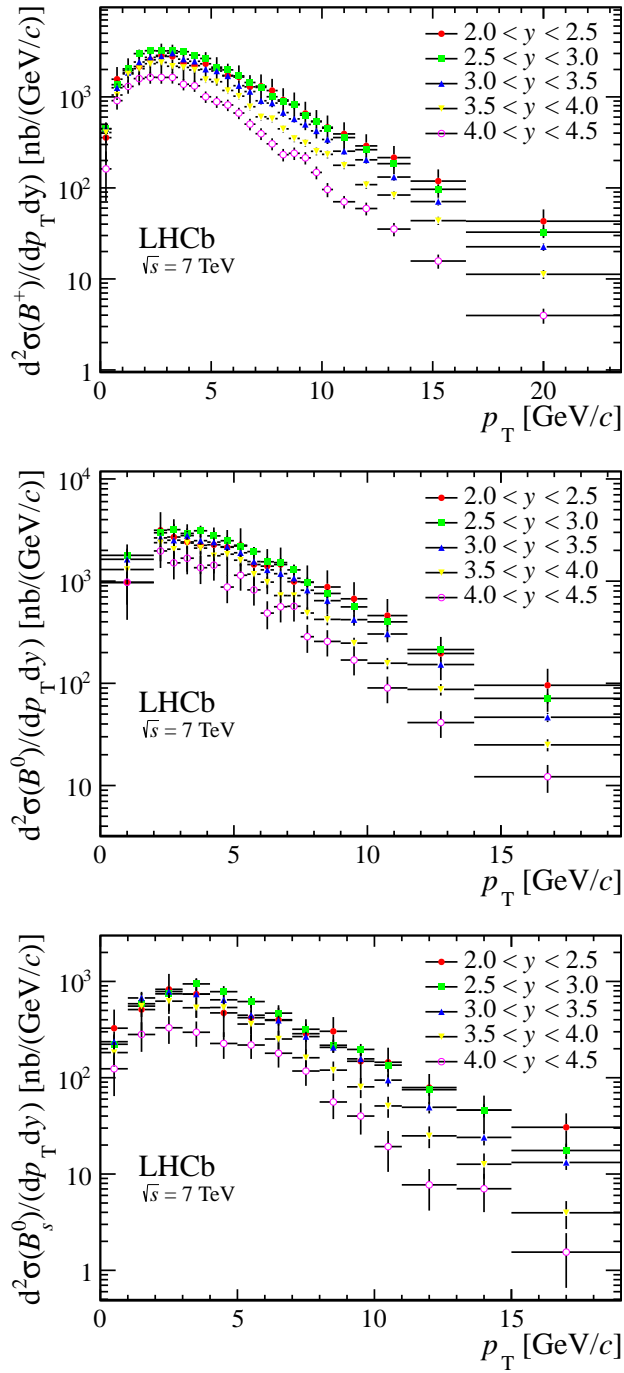


Figure 2: Differential production cross-sections for (*top*) B^+ , (*middle*) B^0 and (*bottom*) B_s^0 mesons, as functions of p_T for each y interval.

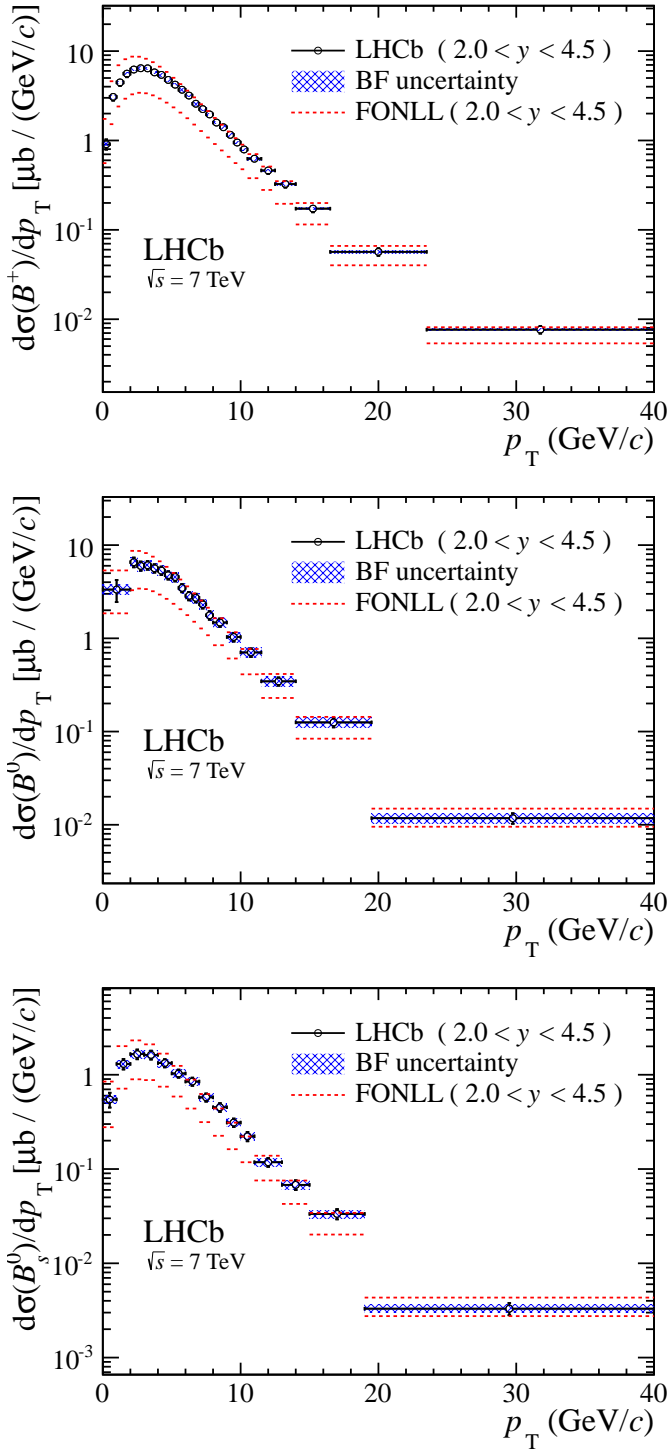


Figure 3: Differential production cross-sections for (top) B^+ , (middle) B^0 and (bottom) B_s^0 mesons, as functions of p_T integrated over the whole y range. The open circles with error bars are the measurements (not including uncertainties from normalisation channel branching fractions and luminosity) and the blue shaded areas are the uncertainties from the branching fractions. The red dashed lines are the upper and lower uncertainty limits of the FONLL computation [3].

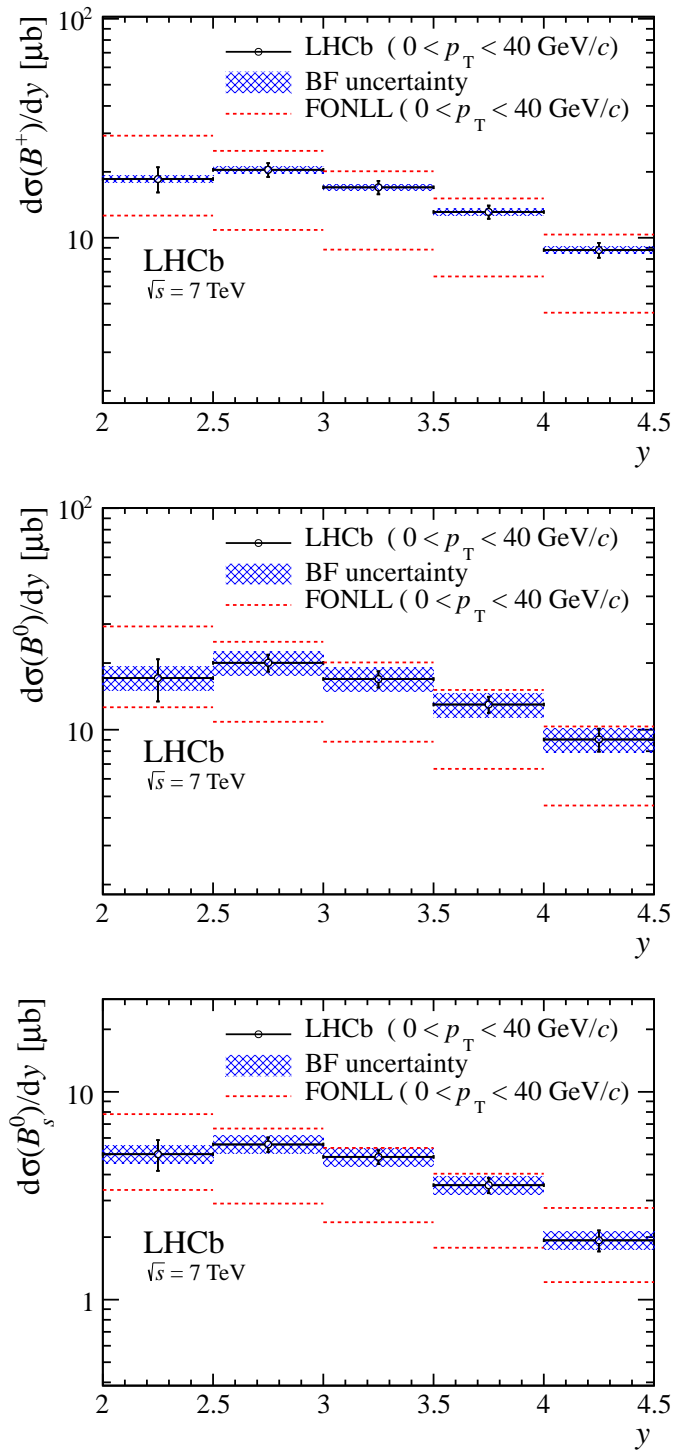


Figure 4: Differential production cross-sections for (*top*) B^+ , (*middle*) B^0 and (*bottom*) B_s^0 mesons, as functions of y integrated over the whole p_T range. The black open circles with error bars are the measurements (not including uncertainties from normalisation channel branching fractions and luminosity) and the blue shaded areas are the uncertainties from the branching fractions. The red dashed lines are the upper and lower uncertainty limits of the FONLL computation [3].

References

- [1] M. Cacciari, M. Greco, and P. Nason, *The p_T spectrum in heavy flavor hadroproduction*, JHEP **05** (1998) 007, [arXiv:hep-ph/9803400](#).
- [2] M. Cacciari, S. Frixione, and P. Nason, *The p_T spectrum in heavy flavor photoproduction*, JHEP **03** (2001) 006, [arXiv:hep-ph/0102134](#).
- [3] M. Cacciari *et al.*, *Theoretical predictions for charm and bottom production at the LHC*, JHEP **10** (2012) 137, [arXiv:1205.6344](#).
- [4] M. Cacciari *et al.*, *QCD analysis of first b cross-section data at 1.96 TeV*, JHEP **07** (2004) 033, [arXiv:hep-ph/0312132](#).
- [5] LHCb collaboration, R. Aaij *et al.*, *Measurement of J/ψ production in pp collisions at $\sqrt{s}=7$ TeV*, Eur. Phys. J. **C71** (2011) 1645, [arXiv:1103.0423](#).
- [6] CMS collaboration, S. Chatrchyan *et al.*, *Measurement of the cross section for production of $b\bar{b} X$, decaying to muons in pp collisions at $\sqrt{s} = 7$ TeV*, JHEP **06** (2012) 110, [arXiv:1203.3458](#).
- [7] LHCb collaboration, R. Aaij *et al.*, *Measurement of $\sigma(pp \rightarrow b\bar{b}X)$ at $\sqrt{s} = 7$ TeV in the forward region*, Phys. Lett. **B694** (2010) 209, [arXiv:1009.2731](#).
- [8] ATLAS collaboration, G. Aad *et al.*, *Measurement of the b -hadron production cross section using decays to $D^*\mu^- X$ final states in pp collisions at $\sqrt{s} = 7$ TeV with the ATLAS detector*, Nucl. Phys. **B864** (2012) 341, [arXiv:1206.3122](#).
- [9] LHCb collaboration, R. Aaij *et al.*, *Measurement of the B^\pm production cross-section in pp collisions at $\sqrt{s}=7$ TeV*, JHEP **04** (2012) 093, [arXiv:1202.4812](#).
- [10] CMS collaboration, V. Khachatryan *et al.*, *Measurement of the B^+ production cross section in pp collisions at $\sqrt{s} = 7$ TeV*, Phys. Rev. Lett. **106** (2011) 112001, [arXiv:1101.0131](#).
- [11] CMS collaboration, S. Chatrchyan *et al.*, *Measurement of the B^0 production cross section in pp collisions at $\sqrt{s} = 7$ TeV*, Phys. Rev. Lett. **106** (2011) 252001, [arXiv:1104.2892](#).
- [12] CMS collaboration, S. Chatrchyan *et al.*, *Measurement of the strange B meson production cross section with $J/\psi\phi$ decays in pp collisions at $\sqrt{s} = 7$ TeV*, Phys. Rev. **D84** (2011) 052008, [arXiv:1106.4048](#).
- [13] LHCb collaboration, A. A. Alves Jr. *et al.*, *The LHCb detector at the LHC*, JINST **3** (2008) S08005.
- [14] R. Aaij *et al.*, *The LHCb trigger and its performance*, JINST **8** (2013) P04022, [arXiv:1211.3055](#).

- [15] Particle Data Group, J. Beringer *et al.*, *Review of particle physics*, Phys. Rev. **D86** (2012) 010001.
- [16] W. D. Hulsbergen, *Decay chain fitting with a Kalman filter*, Nucl. Instrum. Meth. **A552** (2005) 566, [arXiv:physics/0503191](https://arxiv.org/abs/physics/0503191).
- [17] T. Skwarnicki, *A study of the radiative cascade transitions between the Υ' and Υ resonances*, Ph.D. Thesis, DESY-F31-86-02 (1986).
- [18] T. Sjöstrand, S. Mrenna, and P. Skands, *PYTHIA 6.4 physics and manual*, JHEP **05** (2006) 026, [arXiv:hep-ph/0603175](https://arxiv.org/abs/hep-ph/0603175).
- [19] I. Belyaev *et al.*, *Handling of the generation of primary events in GAUSS, the LHCb simulation framework*, Nuclear Science Symposium Conference Record (NSS/MIC) IEEE (2010) 1155.
- [20] D. J. Lange, *The EvtGen particle decay simulation package*, Nucl. Instrum. Meth. **A462** (2001) 152.
- [21] P. Golonka and Z. Was, *PHOTOS Monte Carlo: A precision tool for QED corrections in Z and W decays*, Eur. Phys. J. **C45** (2006) 97, [arXiv:hep-ph/0506026](https://arxiv.org/abs/hep-ph/0506026).
- [22] Geant4 collaboration, J. Allison *et al.*, *Geant4 developments and applications*, IEEE Trans. Nucl. Sci. **53** (2006) 270; Geant4 collaboration, S. Agostinelli *et al.*, *Geant4: a simulation toolkit*, Nucl. Instrum. Meth. **A506** (2003) 250.
- [23] M. Clemencic *et al.*, *The LHCb simulation application, GAUSS: design, evolution and experience*, J. Phys.: Conf. Ser. **331** (2011) 032023.
- [24] M. Adinolfi *et al.*, *Performance of the LHCb RICH detector at the LHC*, Eur. Phys. J. **C73** (2013) 2431, [arXiv:1211.6759](https://arxiv.org/abs/1211.6759).
- [25] LHCb collaboration, R. Aaij *et al.*, *Absolute luminosity measurements with the LHCb detector at the LHC*, JINST **7** (2012) P01010, [arXiv:1110.2866](https://arxiv.org/abs/1110.2866).
- [26] Belle collaboration, K. Abe *et al.*, *Measurements of branching fractions and decay amplitudes in $B \rightarrow J/\psi K^*$ decays*, Phys. Lett. **B538** (2002) 11, [arXiv:hep-ex/0205021](https://arxiv.org/abs/hep-ex/0205021).
- [27] LHCb collaboration, R. Aaij *et al.*, *Amplitude analysis and branching fraction measurement of $\bar{B}_s^0 \rightarrow J/\psi K^+ K^-$* , Phys. Rev. **D87** (2013) 072004, [arXiv:1302.1213](https://arxiv.org/abs/1302.1213).
- [28] LHCb collaboration, R. Aaij *et al.*, *Measurement of b -hadron production fractions in 7 TeV pp collisions*, Phys. Rev. **D85** (2012) 032008, [arXiv:1111.2357](https://arxiv.org/abs/1111.2357).
- [29] LHCb collaboration, R. Aaij *et al.*, *Measurement of the fragmentation fraction ratio f_s/f_d and its dependence on B meson kinematics*, JHEP **04** (2013) 001, [arXiv:1301.5286](https://arxiv.org/abs/1301.5286).

- [30] A. Jaeger *et al.*, *Measurement of the track finding efficiency*, LHCb-PUB-2011-025. CERN-LHCb-PUB-2011-025.
- [31] LHCb collaboration, R. Aaij *et al.*, *Measurement of the CP-violating phase ϕ_s in the decay $B_s^0 \rightarrow J/\psi\phi$* , Phys. Rev. Lett. **108** (2012) 101803, [arXiv:1112.3183](https://arxiv.org/abs/1112.3183).
- [32] P. M. Nadolsky *et al.*, *Implications of CTEQ global analysis for collider observables*, Phys. Rev. **D78** (2008) 013004, [arXiv:0802.0007](https://arxiv.org/abs/0802.0007).